www.lajss.org
Latin American Journal of Solids and Structures 3 (2006) 125–148

An analysis of stress uniformity for viscoelastic materials during SHPB tests

Zhu Jue[a], Hu Shisheng[b] and Wang Lili[*,a,b]

[a]Mechanics and Material Science Research Center, Ningbo University, Ningbo, China
[b]Department of Mechanics & Mechanical Engineering, University of Science & Technology of China, Hefei, China

Abstract

By using characteristics method of viscoelastic wave propagation, the SHPB tests for the viscoelastic materials are numerically studied in the present paper to see how the basic assumption of uniform distribution of stress along the thickness of specimen can be satisfied. It is found that the material parameters such as the relaxation time θ_2 describing the high strain-rate response, the instantaneous wave impedance ratio R_i, and the rise-time of incident wave all markedly influence the stress uniformity, the strain uniformity and the average strain rate of the specimen tested. The results of this study may provide useful theoretical support for the design of a dynamic SHPB test for viscoelastic materials.

Keywords: SHPB, stress uniformity, viscoelastic, characteristics method, high strain rates

1 Introduction

It is well recognized that what distinguishes dynamic response under high strain rates from static response are mainly two so-called dynamic effects, i.e. the inertia effect and the strain rate effect. The former is studied, explicitly or implicitly, by wave propagation in various forms, and the latter has promoted the study of all kinds of nonlinear rate-dependent constitutive relations and failure criteria under an extensive range of strain rates. This is particularly true for polymers, which are more susceptible to strain rate.

The main difficulty is that such two effects are usually coupled. On the one hand, no wave propagation can be analyzed without knowing the corresponding dynamic constitutive relation of material, and consequently the basic characteristics of wave propagation inevitably depend on the strain-rate dependence of mechanical behavior of materials. On the other hand, wave propagation effects should not be neglected in the study of dynamic constitutive relations and failure criteria of materials at high strain rates.

The split Hopkinson pressure bar (SHPB) technique, as schematically shown in Figure 1, has been widely used in studies on the dynamic mechanical behavior of materials at high strain rates

*Corresp. author Email: llwangch@nbu.edu.cn Received 28 Sep 2005; Revised: 3 Nov 2005

($10^2 \sim 10^4 s^{-1}$), since it was firstly proposed by Kolsky in 1949 [1]. Based on two basic assumptions, namely the assumption of one-dimensional stress wave propagation and the assumption of stress uniformity along the specimen thickness, the inertia (wave) effect and the strain-rate effect are cleverly un-coupled in the SHPB technique.

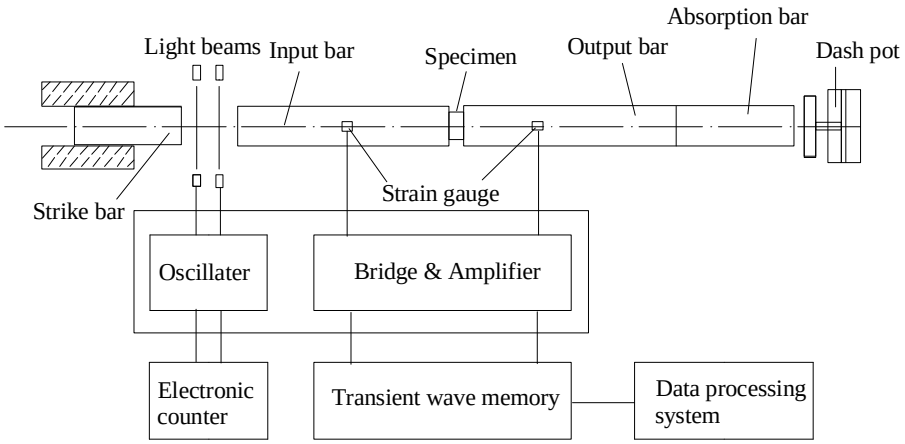

Figure 1: Schematics of the split Hopkinson pressure bar device

According to the theory of one-dimensional elastic waves [2, 6], the incident wave ε_i, the reflected wave ε_r and the transmitted wave ε_t to be measured at the left and right interfaces of the specimen can respectively be measured without wave dispersion at the other positions of the elastic input bar and output bar of SHPB.

On the other hand, according to the assumption of stress uniformity or strain uniformity, we have

$$\sigma_i + \sigma_r = \sigma_t \text{ or } \varepsilon_i + \varepsilon_r = \varepsilon_t \tag{1}$$

where σ_i, σ_r and σ_t (or ε_i, ε_r and ε_t) are the incident, reflected and transmitted stress (strain) respectively. Thus, the dynamic strain rate $\dot{\varepsilon}(t)$, strain $\varepsilon(t)$ and stress $\sigma(t)$ of the short specimen can be determined by

$$\begin{aligned}
\dot{\varepsilon}(t) &= \frac{C_b}{L_0}\left(\varepsilon_i - \varepsilon_r - \varepsilon_t\right) = \frac{2C_b}{L_0}(\varepsilon_i - \varepsilon_t) = -\frac{2C_b}{L_0}\varepsilon_r \\
\varepsilon(t) &= \frac{C_b}{L_0}\int_0^t (\varepsilon_i - \varepsilon_r - \varepsilon_t)dt = \frac{2C_b}{L_0}\int_0^t (\varepsilon_i - \varepsilon_t)dt = -\frac{2C_b}{L_0}\int_0^t \varepsilon_r dt \\
\sigma(t) &= \frac{A_b}{2A_v}E_b\left(\varepsilon_i + \varepsilon_r + \varepsilon_t\right) = \frac{A_b}{A_v}E_b\varepsilon_t = \frac{A_b}{A_v}E_b\left(\varepsilon_i + \varepsilon_r\right)
\end{aligned} \tag{2}$$

where E_b, C_b and A_b are, respectively, the Young's modulus, the elastic wave velocity and the cross-sectional area of the input/output bar; A_v and L_0 are the cross-section area and the

thickness of the specimen, the positive sign (+) denotes the σ and ε in compressive state and the velocity in positive $x-$axis direction.

With regard to the stress uniformity along the specimen thickness (or the dynamic stress equilibrium) in a SHPB test, an incisive and quantitative analysis has been made by Yang and Shim [9], indicating that except for the ratio of wave impedance of the bar and the specimen, the incident pulse shape (such as rectangular, trapezoidal or ramp-rising) also has remarkable effect to the stress uniformity in specimen, although the analysis is limited to an elastic deformation stage of specimens. The dynamic stress equilibrium in relation to soft materials was specially investigated by Song and Chen [4], indicating that in addition to the low wave impedance and low wave speed, specimen thickness and strain rate all influence the stress equilibrium of soft material specimens. However, except Zhou et al [11, 12] who pointed out that the viscoelastic waves propagating in polymer specimen significantly influence the stress uniformity and consequently the data processing of SHPB test, how the viscous character of rate-dependent materials influences the stress uniformity has not been analyzed in detail yet. In fact, as can be seen from a typical oscilloscope record for a viscoelastic specimen in a SHPB test shown in Figure 2, the duration of transmitted pulse is notably longer than that of incident pulse, reflecting the viscous dispersion of the viscoelastic waves propagating in viscoelastic specimen. It will undoubtedly induce a difference between the dynamic stress equilibrium in a viscoelastic specimen and in an elastic specimen.

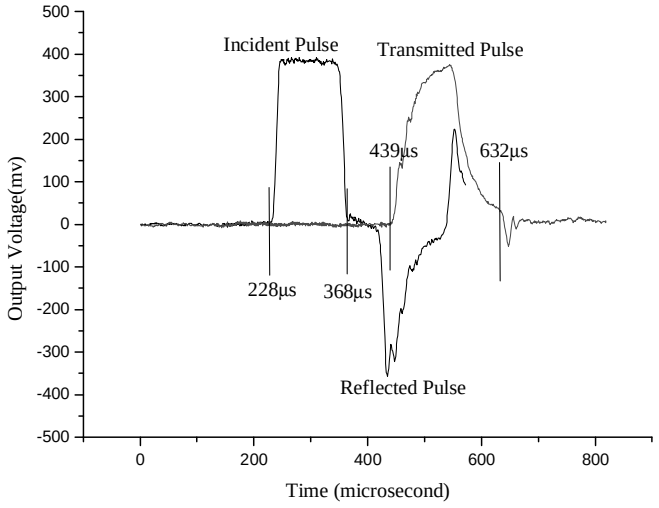

Figure 2: Incident, reflected and transmitted pulses measured for a PMMA specimen in a SHPB test

In the present paper, the SHPB tests for viscoelastic materials are numerically studied by using characteristics method of viscoelastic wave propagation to see how the material relaxation time, the instantaneous wave impedance ratio, as well as the rise-time of incident wave influence

the stress uniformity of viscoelastic specimens.

2 Numerical modeling for characteristics method

A successful numerical study requires a correct constitutive modeling of the relevant materials. Experimental investigation of a variety of polymeric materials at strain-rates from 10^{-4} to $10^{3}s^{-1}$ show that their nonlinear viscoelastic behaviors are well described by the following ZWT (Zhu-Wang-Tang) non-linear viscoelastic constitutive equation [5,8] and its corresponding rheological model is shown in Fig. 3.

$$\sigma = f_e(\varepsilon) + E_1 \int_0^t \dot{\varepsilon}(\tau) \exp(-\frac{t-\tau}{\theta_1}) d\tau + E_2 \int_0^t \dot{\varepsilon}(\tau) \exp(-\frac{t-\tau}{\theta_2}) d\tau, \quad f_e(\varepsilon) = E_0\varepsilon + a\varepsilon^2 + b\varepsilon^3 \tag{3}$$

where, $f_e(\varepsilon)$ describes the nonlinear elastic equilibrium response, E_0, a, b are the corresponding elastic constants; the next integral term describes the viscoelastic response at low strain-rates, E_1, θ_1 are the corresponding elastic constant and relaxation time of the Maxwell element I shown in Fig. 3, the last integral term describes the viscoelastic response at high strain-rates, E_2, θ_2 are the corresponding elastic constant and relaxation time of the Maxwell element II shown in Fig. 3.

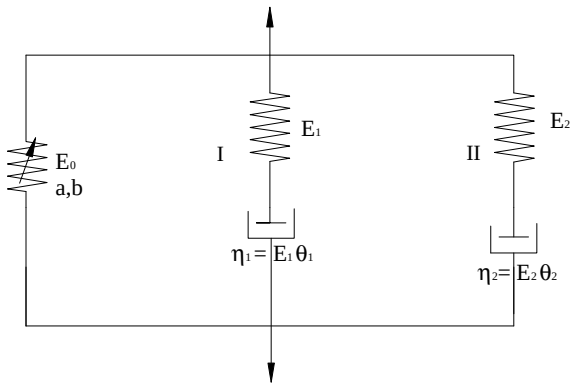

Figure 3: The rheological model corresponding to ZWT equation (3)

Generally, θ_1 is of the order of 5-7 times higher than θ_2 [8], so under impact loading conditions, the low frequency Maxell element I has no enough time to relax until the end of loading, and then it will reduce to a linear spring element with a constant of E_1. Furthermore, the deformation experienced in the dynamic stress equilibrium is generally supposed to be small, so that the second and third terms of $f_e(\varepsilon)$ can be ignored. In other words, the nonlinear spring element in the present case will reduce to a linear spring element with one constant of E_0. Consequently, Eq. (3) reduces to

$$\sigma = E_a\varepsilon + E_2\int_0^t \dot{\varepsilon}(\tau)\exp(-\frac{t-\tau}{\theta_1})d\tau \tag{4a}$$

$$E_a = E_0 + E_1 \tag{4b}$$

Or, equivalently in a differential form

$$\frac{\partial\sigma}{\partial t} + \frac{\sigma}{\theta_2} = (E_a + E_2)\frac{\partial\varepsilon}{\partial t} + \frac{E_a}{\theta_2}\varepsilon \tag{5}$$

Correspondingly, the nonlinear viscoelastic model in Fig. 3 now reduces to a simpler model of three-element linear viscoelastic body or the so-called "standard linear solid" in viscoelastic theory.

The constitutive equation, Eq. (5), together with the following motion equation (6) and continuity equation (7), compose the governing equations for viscoelastic wave in one dimensional stress state.

$$\rho_v\frac{\partial v}{\partial t} = \frac{\partial\sigma}{\partial x} \tag{6}$$

$$\frac{\partial v}{\partial x} = \frac{\partial\varepsilon}{\partial t} \tag{7}$$

where, ρ_v is the density of the specimen.

To solve the governing equations (5)-(7), the characteristics method is especially convenient and effective. To find the characteristics of the present problem, the governing equations (5)-(7) are multiplied by indeterminate coefficients L, M and N, respectively, and then added together as [9]

$$(L+N)\frac{\partial\varepsilon}{\partial t} + \left(M\rho_v\frac{\partial}{\partial t} - L\frac{\partial}{\partial x}\right)v - \left(\frac{N}{E_a+E_2}\frac{\partial}{\partial t} + M\frac{\partial}{\partial x}\right)\sigma + \frac{N}{(E_a+E_2)\,\theta_2}(E_a\varepsilon - \sigma) = 0. \tag{8}$$

In order that the above equation only contains the directional derivatives along the characteristic lines, indeterminate coefficient L, M and N should satisfy the following relations

$$\left.\frac{dx}{dt}\right|_C = \frac{0}{L+N} = -\frac{L}{M\rho_v} = \frac{M(E_a+E_2)}{N}. \tag{9}$$

Obviously, there are two sets of solutions for L, M and N:

$$L + N = 0, \quad \rho_v(E_a+E_2)M^2 = -LN \tag{10a}$$

$$L = M = 0, \quad N \neq 0 \tag{10b}$$

Then from Eq. (8), (9), (10a), we obtain two sets of real characteristics and the corresponding characteristic compatibility relations:

$$\frac{dx}{dt} = \pm\sqrt{\frac{E_a + E_2}{\rho_v}} = C_v \tag{11a}$$

$$dv = \pm\frac{1}{\rho_v C_v}d\sigma \pm \frac{\sigma - E_a\varepsilon}{\rho_v C_v \theta_2}dt = \pm\frac{1}{\rho_v C_v}d\sigma \pm \left[\frac{\sigma - E_a\varepsilon}{(E_a + E_2)\,\theta_2}\right]dx \tag{11b}$$

where "+" is for rightward propagating waves, and "-" is for leftward propagating waves. These sets of characteristics represent the loci of wave fronts propagating with wave velocity C_v, which is determined by the instantaneous response of viscoelastic material. Similarly, from Eq. (8), (9), (10b), we obtain the third set of characteristic and the corresponding compatibility condition along it, respectively, as

$$dx = 0 \tag{12a}$$

$$d\varepsilon - \frac{d\sigma}{(E_a + E_2)} - \frac{\sigma - E_a\varepsilon}{(E_a + E_2)\,\theta_2}dt = 0 \tag{12b}$$

Eq. (12a) coincides with the particle motion locus, and Eq. (12b) is actually another form of the material derivative of viscoelastic constitutive equation (Eq. 5). Note that the terms having dt or dx in the compatibility conditions (Eq. 11b and Eq. 12b) describe the rate-dependence of viscoelastic wave propagation and reflect the dispersion and dissipation characters of viscoelastic waves.

Thus, on the time-space plane tOx, there always exist three characteristics through an arbitrary point. Once the initial-boundary conditions are prescribed, the solution of viscoelastic wave propagation can be solved by the numerical characteristic method, when the difference form is used to replace the differential form for all three sets of characteristics relations.

The same governing equations can also be used to solve the elastic wave propagation in the input bar and output bar, when the Eq. (5) is reduced to Hooke's law by taking θ in this equation as infinite, and consequently all the terms having dt or dx in Eq. (11b) and (12b) will correspondingly vanish.

Now, consider a short viscoelastic specimen with thickness of L_0, which is sandwiched between the input elastic steel bar and the output elastic steel bar (Fig. 1). Assume that a trapezoidal incident pulse with a stress amplitude of σ_0 propagates along the input bar towards the specimen. For convenience, in the following numerical simulation, the reflected waves from the other ends of input and output bar are not considered, and the unloading part of the incident pulse is also not considered, since they are not key factors in the study of stress uniformity, which should be accomplished in the early time of test.

Thus, the trapezoidal pulse is reduced to an incident wave with a linear ramp rising time of τ_s followed by a constant stress amplitude of σ_0, as shown in Fig. 4. In practical numerical

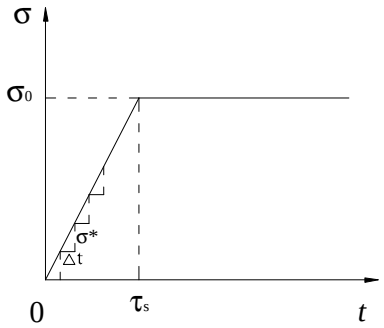

Figure 4: Shape of incident wave propagating in the input bar (boundary condition)

calculation, the linear ramp rising front of incident wave is discretized to a series of ladder-like loading with a stress increment of σ^* per each step, as shown by the dashed lines in Fig. 4.

To investigate the influence of rise-time, introduce the dimensionless rise-time n_s defined as the ratio of the rise-time τ_s and the transit time t_L, which is the time required for a wave to travel from one end to another end of the specimen:

$$n_s = \frac{\tau_s}{t_L} = \frac{\tau_s C_v}{L_0}, \quad t_L = \frac{L_0}{C_v}. \tag{13}$$

To study numerically the stress uniformity of viscoelastic specimen in the present conditions by the characteristics method, actually two categories of computation are involved, namely (1) the computation of "interface points", such as the points M_1, N_1, M_{k+1}, N_{k+1} on the $t-x$ plane shown in Fig. 5(a), and (2) the computation of interior points, such as the points M_2, N_2, M_k, N_k on the $t-x$ plane shown in Fig. 5(a).

The solution at an arbitrary "interface point" at the left interface between the specimen and input bar, for example the point N_1, can be obtained as follows. Through the point N_1, there must exist three characteristic lines: the a_2N_1 from the elastic bar side, and the M_2N_1 and M_1N_1 from the viscoelastic specimen side. Obviously, the following corresponding compatibility relations along those characteristics should be satisfied, namely, along a_2N_1, we have

$$v_e(N_1) - v_2 = \frac{1}{\rho_b C_b} \left[\sigma_e\left(N_1\right) - \sigma_2\right] \tag{14}$$

where ρ_b, C_b are the density and elastic wave velocity of elastic bar respectively. v_e, σ_e are the particle velocity and stress at point N_1 on elastic bar side respectively, and v_2, σ_2 are the particle velocity and stress in region 2 of elastic bar respectively; and along the characteristics

M_2N_1 and M_1N_1, we have respectively,

$$v_{ve}(N_1) - v_{ve}(M_2) = -\frac{1}{\rho_v C_v}\left[\sigma_{ve}(N_1) - \sigma_{ve}(M_2)\right] + \frac{E_a\varepsilon(M_2) - \sigma_{ve}(M_2)}{\rho_v C_v \theta_2}\left[t(N_1) - t(M_2)\right] \tag{15a}$$

$$\varepsilon_{ve}(N_1) - \varepsilon_{ve}(M_1) - \frac{1}{E_a + E_2}\left[\sigma_{ve}(N_1) - \sigma_{ve}(M_1)\right] + \frac{E_a\varepsilon(M_1) - \sigma_{ve}(M_1)}{(E_a + E_2)\theta_2}\left[t(N_1) - t(M_1)\right] = 0 \tag{15b}$$

where v_{ve}, σ_{ve} are the particle velocity and stress at point N_1 on viscoelastic specimen side respectively. Simultaneously, the particle velocity and stress must respectively satisfy the continuity requirement at the interface point N_1 namely,

$$\sigma_e(N_1) = \sigma_{ve}(N_1) \tag{16a}$$

$$v_e(N_1) = v_{ve}(N_1) \tag{16b}$$

Since the solutions at M_1 and M_2 and in region 2 (i.e σ_2 and v_2) are all known, the particle velocity $v_{ve}(N_1)$, stress $\sigma_{ve}(N_1)$ and strain $\varepsilon_{ve}(N_1)$ can be solved by Eq. (14), (15a,b), (16a,b), and are correspondingly illustrated on the σ-v plane, as shown in Fig. 5(b).

Similarly, the solutions of an arbitrary point N_{k+1} at the right interface between the specimen and output bar can be obtained by the following relations, namely, the characteristic compatibility relations along N_kN_{k+1} and $N_{k+1}M_{k+1}$ from viscoelastic specimen side

$$v_{ve}(N_{k+1}) - v_{ve}(N_k) = \frac{1}{\rho_v C_v}\left[\sigma_{ve}(N_{k+1}) - \sigma_{ve}(N_k)\right] - \frac{E_a\varepsilon_{ve}(N_k) - \sigma_{ve}(N_k)}{\rho_v C_v \theta_2}\left[t(N_{k+1}) - t(N_k)\right] \tag{17a}$$

$$\begin{aligned}\varepsilon_{ve}(N_{k+1}) - \varepsilon_{ve}(M_{k+1}) - \frac{1}{E_a + E_2}\left[\sigma_{ve}(N_{k+1}) - \sigma_{ve}(M_{k+1})\right] + \\ \frac{E_a\varepsilon_{ve}(M_{k+1}) - \sigma_{ve}(M_{k+1})}{(E_a + E_2)\theta_2}\left[t(N_{k+1}) - t(M_{k+1})\right] = 0\end{aligned} \tag{17b}$$

as well as the characteristic compatibility relation along $N_{k+1}M_{k+2}$ from elastic output bar side:

$$v_e(N_{k+1}) - v_e(M_{k+2}) = -\frac{1}{\rho_b C_b}\left[\sigma_e(N_{k+1}) - \sigma_e(M_{k+2})\right] \tag{18}$$

Furthermore, the continuity requirement for the particle velocity and the stress across the right interface of specimen provides:

$$v_{ve}(M_{k+1}) = v_e(M_{k+1}) \tag{19a}$$

$$\sigma_{ve}(M_{k+1}) = \sigma_e(M_{k+1}) \tag{19b}$$

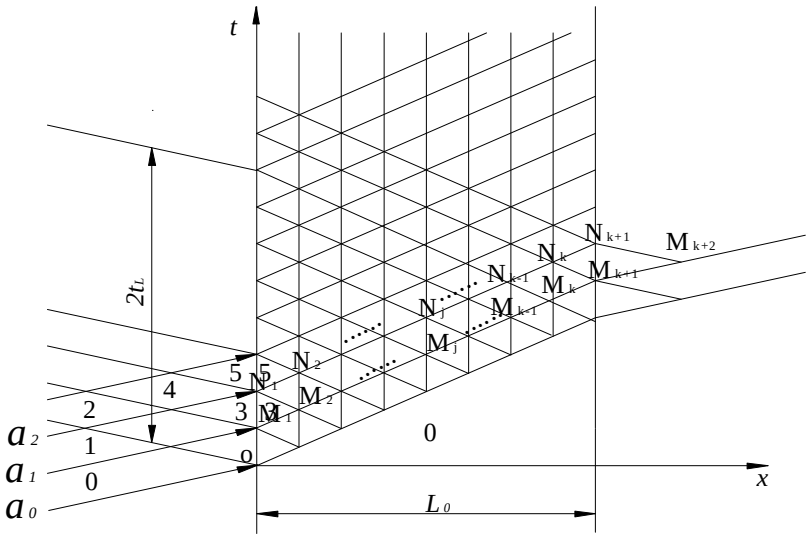

(a) Characteristics on t-x plane (physical plane)

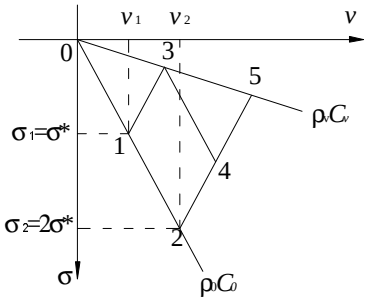

(b) Characteristics on σ-v plane (velocity plane)

Figure 5: Solution of wave propagation in SHPB test for viscoelastic specimen by characteristics method

Note that the waves propagating rightwards along the elastic output bar are elastic simple waves, so we have

$$v_e\left(M_{k+2}\right) = v_e\left(M_{k+1}\right) \tag{20a}$$

$$\sigma_e\left(M_{k+2}\right) = \sigma_e\left(M_{k+1}\right) \tag{20b}$$

Thus, from Eq. (17a,b), (18), (19a,b) and (20a,b), the solution at the right interface point N_{k+1}, $\sigma_{ve}(N_{k+1})$, $v_{ve}(N_{k+1})$ and $\varepsilon_{ve}(N_{k+1})$, can be solved.

On the other hand, the solutions at an arbitrary "interior point", for example the point N_2, can be solved as follows. Through the point N_2, there must exist three characteristic lines, N_1N_2, N_2M_3 and N_2M_2. Obviously, the following three characteristic compatibility relations

respectively along these characteristics should be satisfied [7]:

$$\begin{aligned}
v_{ve}(N_2) - v_{ve}(N_1) &= \frac{1}{\rho_v C_v}\left[\sigma_{ve}(N_2) - \sigma_{ve}(N_1)\right] - \frac{E_a\varepsilon_{ve}(N_1) - \sigma_{ve}(N_1)}{\rho_v C_v \theta_2}\left[t(N_2) - t(N_1)\right] \\
v_{ve}(N_2) - v_{ve}(M_3) &= -\frac{1}{\rho_v C_v}\left[\sigma_{ve}(N_2) - \sigma_{ve}(M_3)\right] + \frac{E_a\varepsilon_{ve}(M_3) - \sigma_{ve}(M_3)}{\rho_v C_v \theta_2}\left[t(N_2) - t(M_3)\right] \\
\varepsilon_{ve}(N_2) - \varepsilon_{ve}(M_2) &= \frac{1}{E_a + E_2}\left[\sigma_{ve}(N_2) - \sigma_{ve}(M_2)\right] - \frac{E_a\varepsilon_{ve}(M_2) - \sigma_{ve}(M_2)}{(E_a + E_2)\theta_2}\left[t(N_2) - t(M_2)\right]
\end{aligned} \tag{21}$$

Thus, the unknown $\sigma_{ve}(N_2)$, $v_{ve}(N_2)$ and $\varepsilon_{ve}(N_2)$, can be determined.

3 Analysis on stress uniformity of viscoelastic materials in SHPB tests

From Eq. (11) it can be seen that the characters of viscoelastic wave are dependent on the instantaneous wave impedance $\rho_v C_v$ and the relaxation time θ_2, which should also influence the stress uniformity of viscoelastic specimen in SHPB test. Furthermore, as pointed out in [9] and [4], the incident wave shape (or substantially the rise time τ_s of incident wave front) may influence the stress uniformity too. Thus, in addition to the dimensionless rise-time n_s defined in Eq. (13), another dimensionless parameter is introduced, namely, the dimensionless generalized wave impedance ratio R_i, defined as

$$R_i = \frac{A_b \rho_b C_b}{A_v \rho_v C_v}, \tag{22}$$

where A is the cross-section area, the subscripts b and v denote the quantities of the elastic bar and the viscoelastic specimens respectively. Therefore, in the following numerical analyses, we will mainly study how the relaxation time θ_2, the dimensionless rise-time τ_s/t_L and the dimensionless instantaneous wave impedance ratio R_i influence the stress uniformity.

The material parameters used in numerical simulation are $\rho_b = 7.8 \times 10^3$ kg/m^3, $E_b = 210$ GPa for elastic steel bar, and those listed in Table 1 for viscoelastic specimens. The material $VE1$ in Table 1 represents a grade of PMMA, of which all parameters were experimentally determined as reported in [7], but the area ratio A_b/A_v is adjusted to round up R_i as an integer 15. In order to see how the relaxation time θ_2 influence the stress uniformity, we assume two materials: one is material $VE2$, of which the only difference from $VE1$ is that the θ_2 for $VE2$ is only a tenth of that for $VE1$; another is material EL, of which the only difference from $VE1$ is that its θ_2 is infinitive, namely equivalent to an elastic specimen. Moreover, we assume a material $VE3$, of which the only difference from $VE1$ is that its instantaneous wave impedance ratio is a third of that of $VE1$, in order to see how the wave impedance ratio R_i influence the stress uniformity of viscoelastic specimens. The thickness of all specimens is adopted as L_0 =10mm.

Table 1: The ZWT parameters of representative materials

material	ρ_v(kg/m^3)	E_0(GPa)	E_1(GPa)	E_2(GPa)	$\theta_2(\mu s)$	R_i
VE1	1.19×10^3	2.04	0.897	3.07	95.4	15
VE2	1.19×10^3	2.04	0.897	3.07	9.54	15
*VE*3	1.19×10^3	20.4	8.97	30.7	95.4	5
EL	1.19×10^3	2.04	0.897	3.07	∞	15

In the case of rise-time $\tau_s/t_L = 1$, the curves of dimensionless stress σ/σ_w versus time t/t_L on the left and right interface of specimens for different material $VE1$, $VE2$ and EL are respectively shown in Fig. 6(a, b), and the comparisons of those are shown in Fig. 6(c). As can be seen from those curves, the stress-time curves for viscoelastic specimens all display attenuation character, and such attenuation can be observed not only from the whole curve but also from each step of stress-time curve. Obviously, the relaxation time does influences the stress wave profile in specimen, and consequently the stress distribution along specimen thickness, although the stress difference between the left and right interface of specimen become smaller after several forth-back wave propagating in specimen, and then tends towards the stress uniformity (Fig. 6c). A further comparisons show that the smaller the relaxation time θ_2 is, the lower the stress and the stress rate are. So it is clear that the analysis of stress uniformity based on elastic waves does not represent the situation of stress uniformity of viscoelastic specimen at all.

For other three different rise-times $\tau_s/t_L = 2$, 4, 10, the stress-time curves of specimens with different θ_2 calculated at the left and right interfaces of specimen are shown in Fig. 7-Fig. 9. Comparing Fig. 6-9 with each other, it can be seen that both the dimensionless stress-difference between left and right interfaces $\frac{\Delta\sigma}{\sigma_0} = \left[\frac{\sigma_L}{\sigma_0} - \frac{\sigma_R}{\sigma_0}\right]$ and the dimensionless stress-rate $\frac{\partial(\sigma/\sigma_0)}{\partial t}$ decrease with the increase of the dimensionless rise-time τ_s/t_L, except for $\tau_s/t_L = 1$.

For two different rise-times $n_s = \tau_s/t_L = 1$, 10, the stress-time curves of specimens with different R_i (=15, 5) calculated at the left and right interfaces of specimen are shown in Fig. 10 and Fig. 11. It can be seen that the dimensionless instantaneous wave impedance ratio R_i does influence markedly the stress uniformity, although such influence is different for different rise time. In the case of $\tau_s/t_L = 1$, the viscoelastic specimen with $R_i = 5$ reaches the stress uniformity earlier than that with $R_i = 15$ (Fig. 10), while in the case of $\tau_s/t_L = 10$, contrarily, the viscoelastic specimen with $R_i = 5$ reaches the stress uniformity later than that with $R_i = 15$ (Fig. 11), since the dimensionless stress difference $\Delta\sigma/\sigma_0$ decreases with the increase of rise-time τ_s/t_L.

To evaluate quantitatively the approximity of stress uniformity in viscoelastic specimen, similar to the suggestion in [12], [3] and [10], a dimensionless stress uniformity parameter α_k is introduced, which is defined as the ratio of the stress difference $(\sigma_L - \sigma_R)$ between the left and

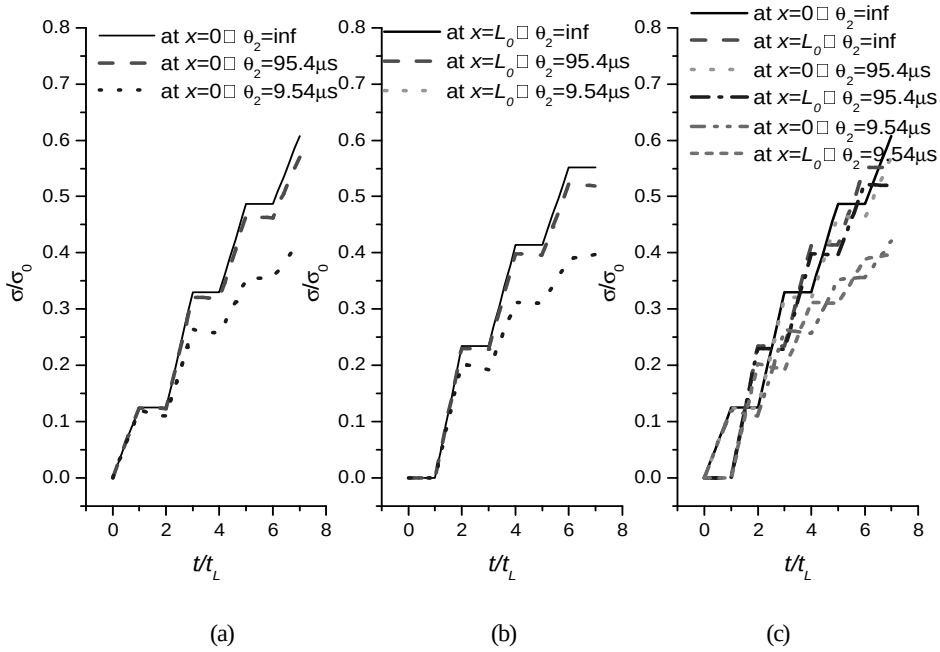

Figure 6: Dimensionless stress-time curves of specimens $VE1$, $VE2$ and EL with different relaxation time $\theta_2$under the incident waves with rise-time of $\tau_s/t_L = 1$

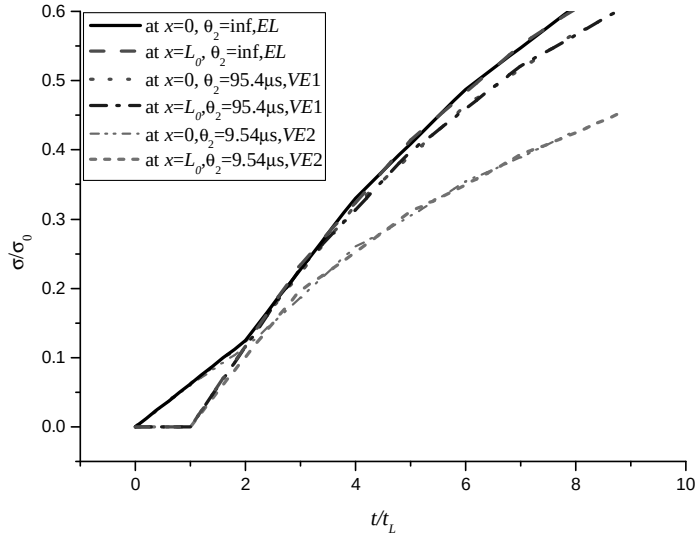

Figure 7: Dimensionless stress-time curves of specimens $VE1$, $VE2$ and EL with different relaxation time θ_2 under the incident waves with rise-time of $\tau_s/t_L = 2$

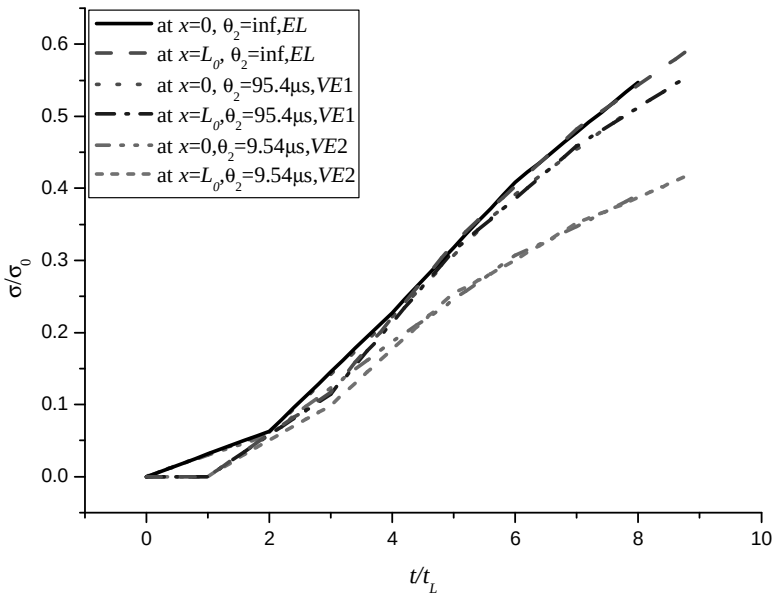

Figure 8: Dimensionless stress-time curves of specimens $VE1$, $VE2$ and EL with different relaxation time θ_2 under the incident waves with rise-time of $\tau_s/t_L = 4$

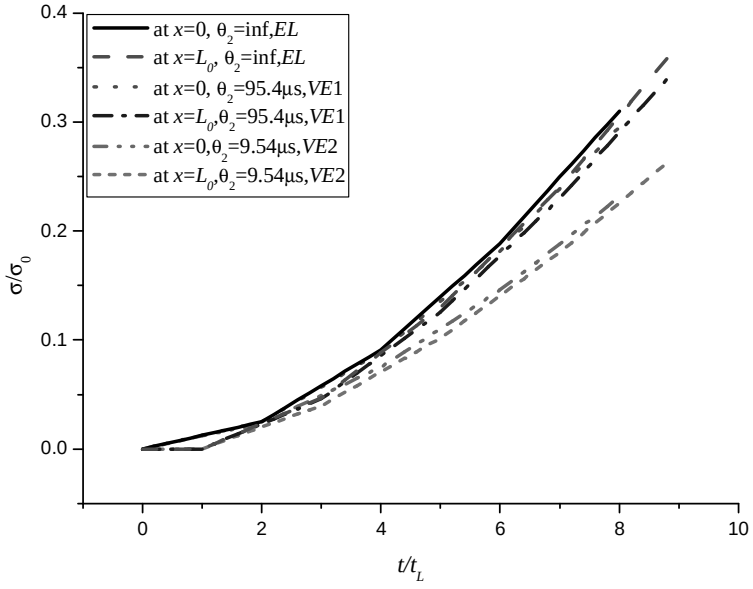

Figure 9: Dimensionless stress-time curves of specimens $VE1$, $VE2$ and EL with different relaxation time θ_2 under the incident waves with rise-time of $\tau_s/t_L = 10$

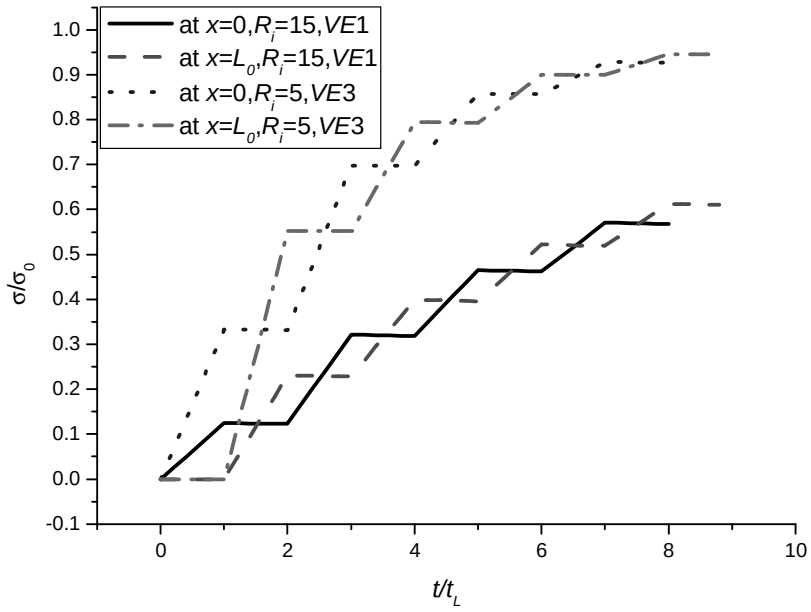

Figure 10: Dimensionless stress-time curves of $VE1$ and $VE3$ with different wave impedance ratios R_i, in the case of the incident waves with rise-time of $\tau_s/t_L = 1$

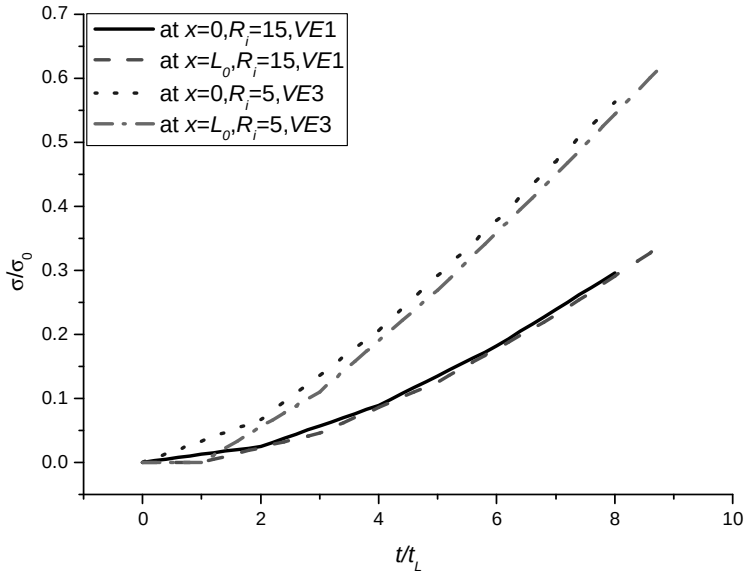

Figure 11: Dimensionless stress-time curves of $VE1$ and $VE3$ with different wave impedance ratios R_i, in the case of the incident waves with rise-time of $\tau_s/t_L = 10$

the right interface and their average

$$\alpha_k = \left| \frac{\sigma_L(t) - \sigma_R(t)}{(\sigma_L(t) + \sigma_R(t))/2} \right| \tag{23}$$

if $\alpha_k \leq 5\%$ at $t \geq t_u$, then the t_u is approximately defined as the beginning time of stress uniformity, or, a dimensionless beginning time of stress uniformity (non-integer) can be defined as

$$\bar{t}_u = n_u = t_u/t_L \tag{24}$$

where the n_u is the number of wave propagation between two interfaces of the specimen before the stress uniformity reaches.

With regard to the stress uniformity of elastic specimen, when rise-time $\tau_s/t_L = 2$, the following accurate theoretical formula was deduced by Yang and Shim [9]:

$$\alpha_k = \frac{2\beta^2(1-\beta)^{k-2}}{(1+\beta)^k + (1-\beta)^{k-2}} = \frac{2(1/R_i)^2(1-1/R_i)^{k-2}}{(1+1/R_i)^k + (1-1/R_i)^{k-2}} \quad for \quad k > 2 \tag{25}$$

Where the integer k is the traversing number of wave propagating in specimen, the β in Eq. (25) used in [9] is just the reciprocal of R_i defined in Eq. (22).

For viscoelastic specimen $VE1$ and $VE2$ with different relaxation time, how the stress uniformity parameter α_k varies with the wave transiting number t/t_L at different rise-times is calculated by the characteristics numerical method mentioned above and shown in Fig. 12. The results predicted by Eq. (25) for elastic specimen EL at $\tau_s = 2t_L$ are given in the same figure too. By comparing those calculated curves, it is clear that concerning on the approximity of stress uniformity, whatever the relaxation time is 95.4 μs or 9.54 μs, the incident wave with the shortest rise time $\tau_s/t_L = 1$ displays the worst situation, especially during the early loading period, while the incident wave with rise time of $\tau_s/t_L = 2$ displays the best situation. A further longer rise-time will unexpectedly deteriorate the stress uniformity. This conclusion qualitatively coincides with the results given by Yang and Shim [9] for the SHPB specimen in an elastic deformation stage.

For viscoelastic specimen $VE1$ and $VE3$ with different wave impedance ratios R_i, how the stress uniformity parameter α_k varies with the wave transiting number t/t_L at different rise-times is calculated by the characteristics numerical method mentioned above and shown in Fig. 13. The results predicted by Eq. (25) for elastic specimen EL at $\tau_s = 2t_L$ are given in the same figure too. It is also shown that whatever the R_i is 15 or 5, the incident wave with the shortest rise time $\tau_s/t_L = 1$ displays the worst situation, while the incident wave with rise time of $\tau_s/t_L = 2$ displays the best situation. A further longer rise-time will unexpectedly deteriorate the stress uniformity.

The numerical results of dimensionless stress uniformity time n_u for specimens of different materials under different rise-time loading are collected together in Table 2. It reveals again that except for $\tau_s/t_L = 1$, the n_u for all material concerned increases with the increase of rise-times

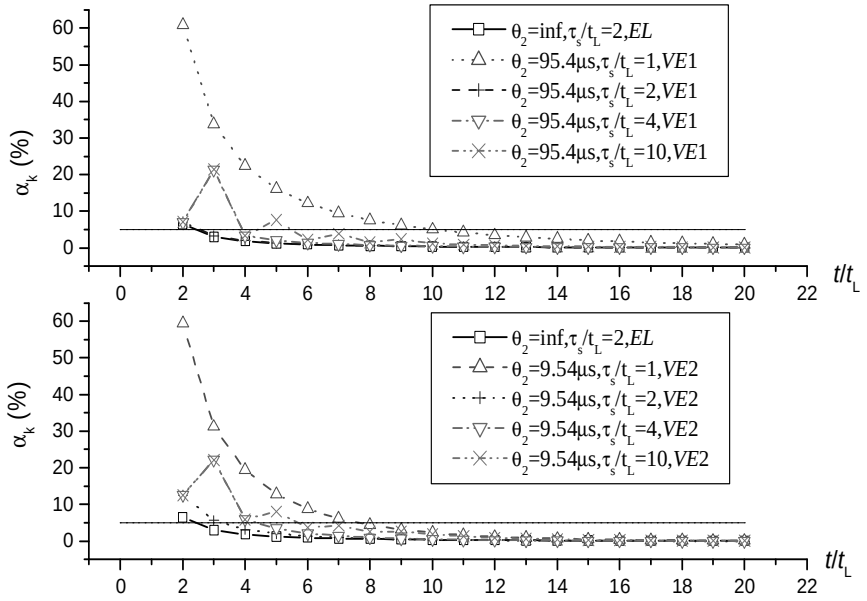

Figure 12: Relation between α_k and t/t_L for specimen $VE1$ and $VE2$ at different rise-times

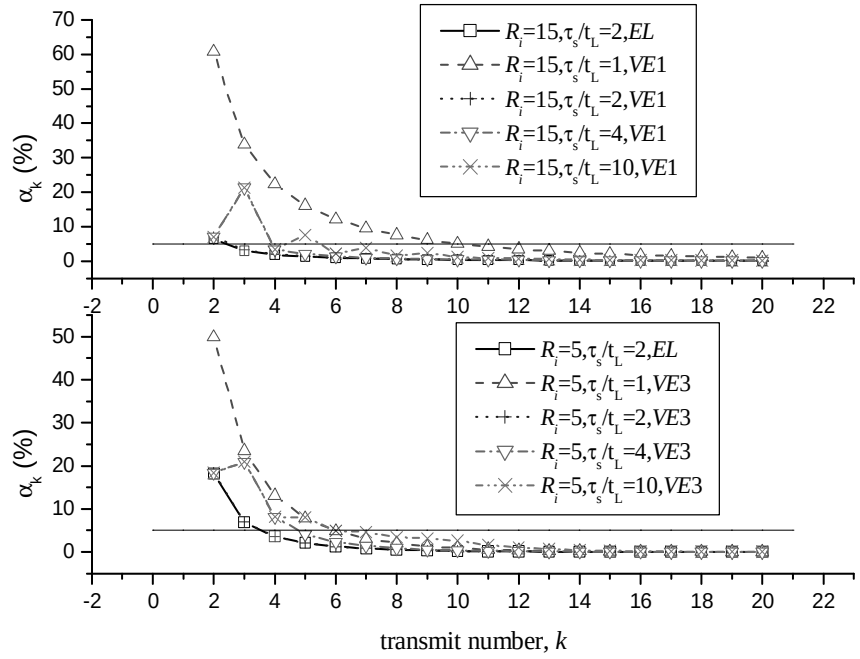

Figure 13: Relation between α_k and t/t_L for specimen $VE1$ and $VE3$ at different rise-times

τ_s/t_L. Moreover, as can be seen by the comparison of $VE1$ and $VE2$, except for $\tau_s/t_L = 1$, the n_u increases with the decrease of relaxation rime θ_2, In other words, the approximity of stress uniformity become worse with decreasing θ_2, so that the viscous effect on the stress uniformity should be taken into account particularly for the viscoelastic materials with low θ_2. On the other hand, from the comparison of $VE1$ and $VE3$, it can be seen that, expect for $\tau_s/t_L = 1$, the n_u increases with the decrease of the wave impedance ratio R_i. However, it is worthwhile noticing that at a certain combination of θ_2 and R_i, for example for the viscoelastic specimen $VE1$, its stress uniformity character is nearly the same as that for the corresponding elastic specimen EL. Only in such situation, the influence of viscous character of viscoelastic materials on the stress uniformity can be disregarded.

Table 2: The n_u required for stress uniformity for different specimens at different rise-times of incident waves.

n_u	$\tau_s = t_L$	$\tau_s = 2t_L$	$\tau_s = 4t_L$	$\tau_s = 10t_L$
EL $\theta_2 = \infty$, $R_i = 15$	10.2	2.2	4.0	5.4
$VE1$ $\theta_2 = 95.4\mu s$, $R_i = 15$	10.2	2.2	4.0	5.4
$VE2$ $\theta_2 = 9.54\mu s$, $R_i = 15$	7.2	3.2	4.2	5.8
$VE3$ $\theta_2 = 95.4\mu s$, $R_i = 5$	5.4	3.2	4.4	6.0

4 Analysis on strain uniformity of viscoelastic materials in SHPB tests

Obviously, in linear elastic analyses, a proportional relation always exists between the stress wave and strain wave, and consequently, a "stress uniformity" assumption is actually equivalent to a "strain uniformity" assumption, as expressed by Eq. (1). However, in viscoelastic analyses, such a proportional relation no longer exists due to the viscous dispersion. For example, when a constant-velocity loading is suddenly applied to one end of a viscoelastic bar, the stress profile of viscoelastic wave propagating along the bar displays a relaxation character, while the strain profile of viscoelastic wave displays a creep character [7]. It means that in SHPB tests for viscoelastic specimens, not only the stress uniformity but also the strain uniformity should be inspected, to provide the guideline for assessing the validity of experimental results.

The strain-time curves calculated σ or specimens $VE1$, $VE2$ and EL at $\sigma_0 = 650$ MPa are shown in Fig. 14 and Fig. 15 respectively for two different rise-times $\tau_s/t_L = 1$ and 10. As can be seen, contrary to the stress-time curves shown in Fig. 6-9, where the stress-time curves of

viscoelastic specimens are lower than that of elastic specimen, the strain-time of specimen $VE1$ is higher than that of specimen EL, and the strain-time curve of specimen $VE2$ is further higher than that of specimen $VE1$. It means that due to the viscous effect, the smaller the θ_2 is, the larger the rheological deformation of specimen will be.

To evaluate quantitatively the approximity of strain uniformity, a parameter γ_k is introduced which is defined as the ratio of the strain difference $(\varepsilon_L - \varepsilon_R)$ between the left and right interfaces and their average

$$\gamma_k = \left| \frac{\varepsilon_L(t) - \varepsilon_R(t)}{(\varepsilon_L(t) + \varepsilon_R(t))/2} \right| \tag{26}$$

Again, if $\gamma_k \leq 5\%$ at $t \geq t_u$, then t_u is regarded as the beginning of strain uniformity, and the $\bar{t}_u$ $(=n_u)$ defined in Eq. (24) is regarded as the dimensionless beginning time of strain uniformity (or the wave traversing times for reaching strain uniformity).

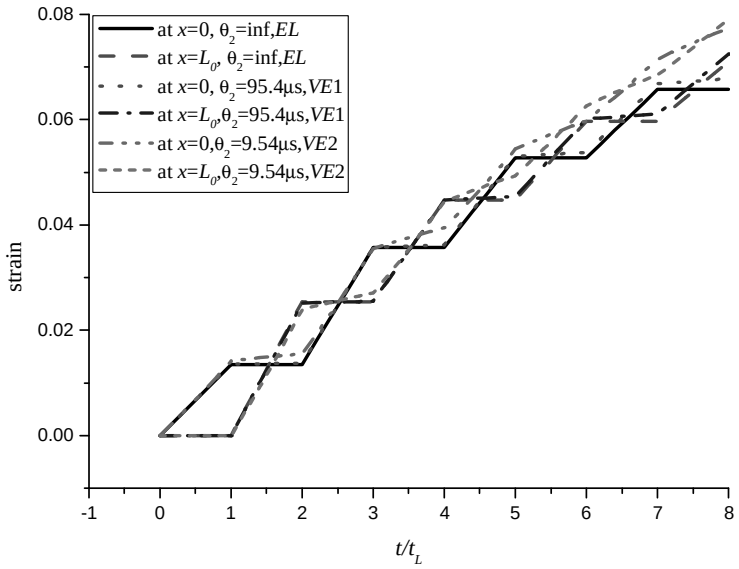

Figure 14: Strain-time curves of specimens $VE1$, $VE2$ and EL with different relaxation time θ_2 in the case of the incident waves with rise-time of $\tau_s/t_L = 1$

The numerical results of how the strain uniformity parameter γ_k varies with τ_s/t_L, θ_2, R_i, and how the dimensionless beginning time of strain uniformity n_u varies with τ_s/t_L, θ_2, R_i, calculated for specimens $VE1$, $VE2$, $VE3$ and EL are given in Fig. 16 and Table 3, respectively. Comparing the Fig. 16 with Fig. 12, and the Table 3 with Table 2, it can be seen that the strain uniformity in general does not coincide with the stress uniformity, except for elastic specimen EL as could be expected. Comparing the results for the viscoelastic specimens $VE1$ and $VE2$, it can be seen that when θ_2 decreases from 95.4 μs to 9.54 μs, the specimen reaches the state of strain uniformity earlier than that of stress uniformity if the rise-time is shorter. However, the situation transfers to the contrary if the rise-time becomes longer. On the other hand, by

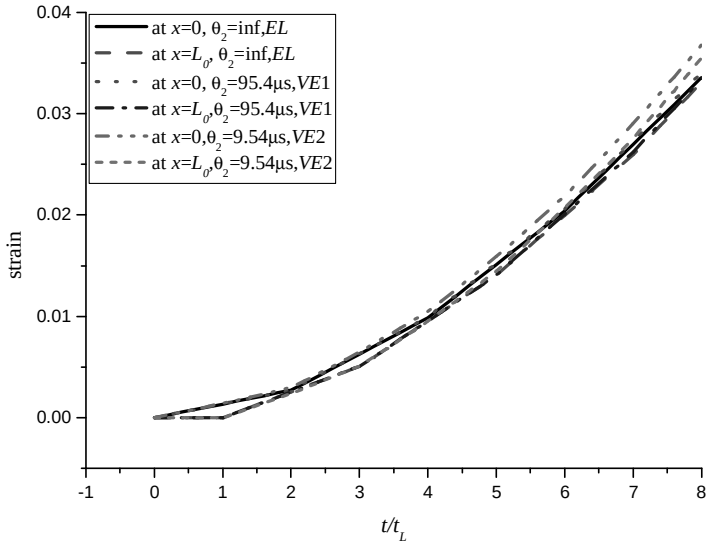

Figure 15: Strain-time curves of specimens $VE1$, $VE2$ and EL with different relaxation time θ_2 in the case of the incident waves with rise-time of $\tau_s/t_L = 10$

comparing the results for specimens $VE1$ and $VE3$, it can be seen that when R_i decreases from 15 to 5, the specimen reaches the state of strain uniformity later than that of stress uniformity, if the rise-time increases to $\tau_s/t_L = 10$. Thus, when viscoelastic materials are tested by SHPB technique, more attention should be paid to strain uniformity besides stress uniformity, and experiment data must satisfy both of uniformity requirement.

Table 3: The n_u required for strain uniformity for different specimens at different rise-times of incident waves.

n_u	$\tau_s = t_L$	τ_s=$2t_L$	τ_s=$4t_L$	τ_s=$10t_L$
EL, $\theta_2 = \infty$, R_i=15	10.2	2.2	4.0	5.4
$VE1$, $\theta_2 = 95.4\mu$s, R_i=15	9.2	2.2	4.0	5.6
$VE2$, $\theta_2 = 9.54\mu$s, R_i=15	5.4	2.8	4.4	7.2
$VE3$, $\theta_2 = 95.4\mu$s, R_i=5	5.4	3.2	4.4	6.4

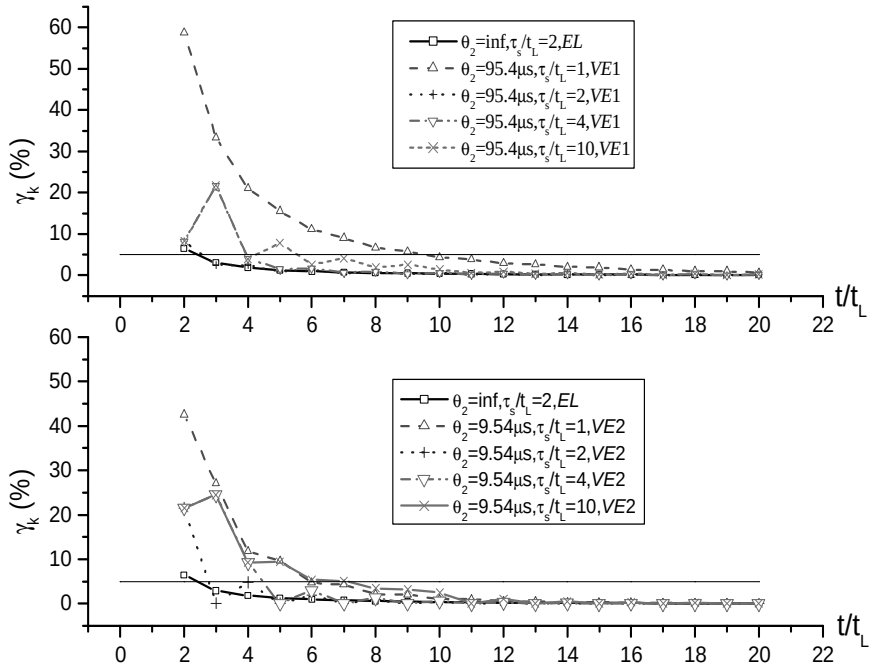

Figure 16: The relation between γ_k and t/t_L for specimen $VE1$ and $VE2$ at different rise-times.

5 Analysis on average strain rate of visco-elastic materials in SHPB tests

The most basic aim of SHPB test is to study the material behavior under high strain rates. For conventional SHPB technique, the strain rate is determined by (see Eq. 2):

$$\dot{\varepsilon}(t) = \frac{(v_r(t) - v_l(t))}{L_0} \tag{27}$$

where, the subscripts l and r denote respectively the particle velocity v at the left and right interfaces of the specimen. Taking the specimen $VE1$ as an example, the calculated particle velocity-time curves for the left interface, middle section and right interface are given in Fig. 17. The vertical line of $t = t_u$ is also plotted on the same figure for reference, showing the beginning time of stress uniformity. It can be seen that the velocity distribution along the thickness of specimen is non-uniform, particularly before $t = t_u$.

On the other hand, the particle strain rate can be directly calculated by the time-differential of strain:

$$\dot{\varepsilon}(t) = \frac{d\varepsilon(t)}{dt} \tag{28}$$

For the specimen $VE1$ the strain rate-time curves respectively determined by Eq. (27) and (28) are given in Fig. 18 for different rise-times, showing the non-uniform distribution of strain

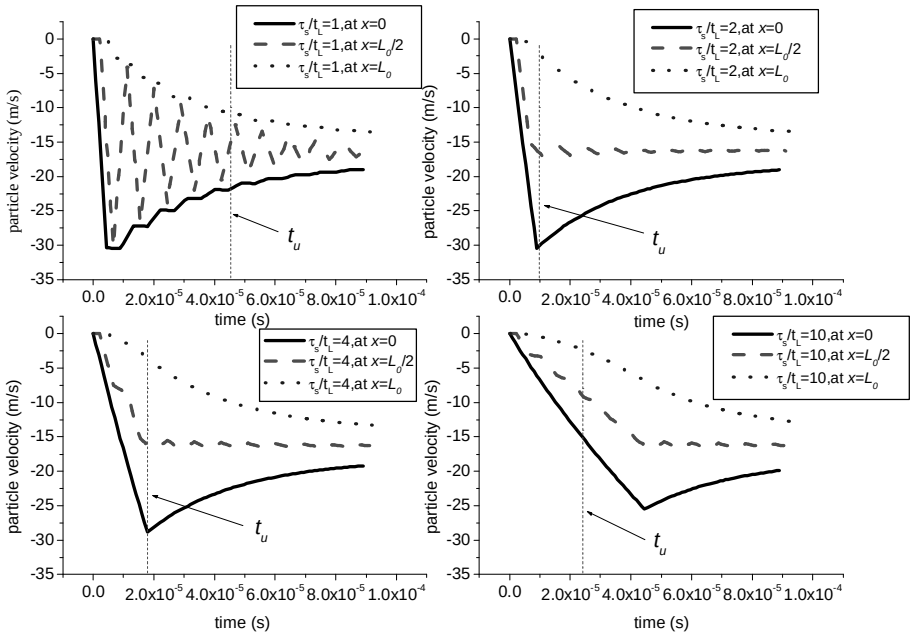

Figure 17: Particle velocity-time curves of $VE1$ for different rise-times of (a)$\tau_s/t_L = 1$ (b)$\tau_s/t_L = 2$, (c)$\tau_s/t_L = 4$, (d)$\tau_s/t_L = 10$

rate in viscoelastic specimen. The vertical line of $t = t_u$ is also plotted on the same figure for reference, showing the beginning time of stress uniformity. It can be seen that the non-uniformity of strain rate decreases with increasing rise-time, particularly after the stress-uniformity reaches ($t = t_u$). Note that the strain rate calculated by Eq. (27) almost coincides with that calculated by Eq.(28) at the middle section $x = L_0/2$, which actually represents the average strain rate of specimen. Expect for the case of longer rise-time ($\tau_s/t_L = 10$), the average strain rates after $t = t_u$ all decrease with time. The average strain rates for different specimens at different τ_s/t_L are listed in Table 4. It is not difficult to find that the strain rate increases with decreasing θ_2, but decreases with decreasing R_i and decreases with increasing τ_s/t_L, namely, the strain rate is not only dependent on the relaxation time θ_2 and the wave impedance ratio R_i but also on the rise-time of incident wave τ_s/t_L. Those factors should be considered in design of SHPB experiments.

6 Conclusions

From the above numerical analyses by using characteristics method of viscoelastic wave propagation, obviously, the following main points with regard to the stress uniformity for viscoelastic materials during SHPB tests can be concluded.

Table 4: The average strain rate at $t = t_u$ for different specimens at different rise-times of incident waves

average strain rate ($10^3 s^{-1}$)	τ_s/t_L=1	τ_s/t_L=2	τ_s/t_L=4	τ_s/t_L=10
EL, $\theta_2 = \infty$, R_i=15		1.11		
$VE1$, $\theta_2 = 95.4\mu s$, R_i=15	1.29	1.27	1.25	1.14
$VE2$, $\theta_2 = 9.54\mu s$, R_i=15	1.67	1.65	1.60	1.43
$VE3$, $\theta_2 = 95.4\mu s$, R_i=5	0.422	0.419	0.415	0.406

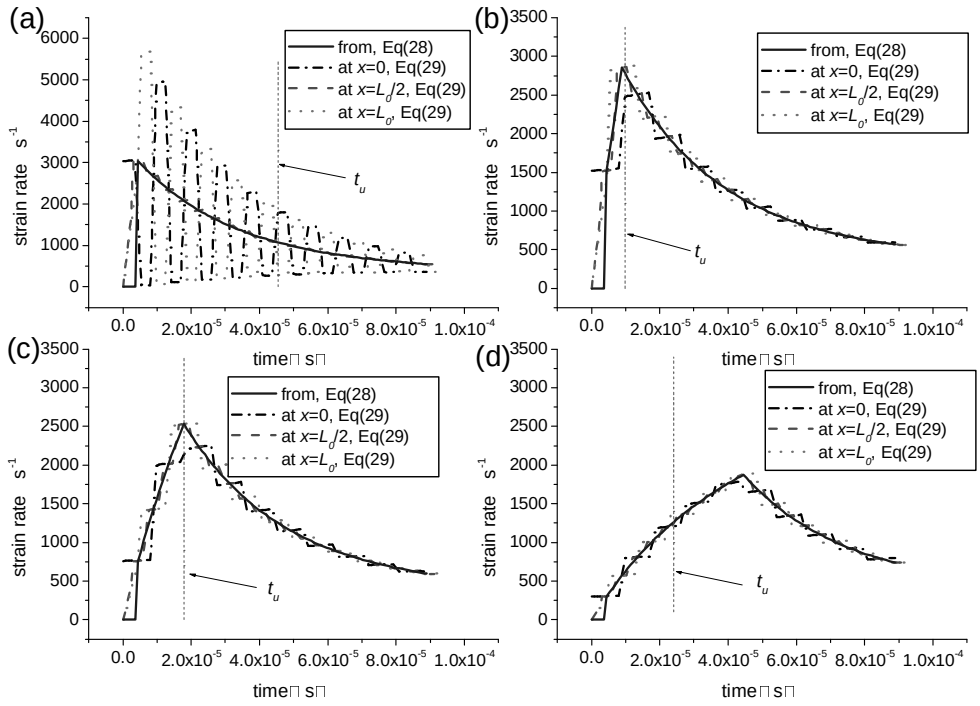

Figure 18: Strain rate-time curves calculated by Eq. (27) and Eq. (28) for different rise-times of (a)$\tau_s/t_L = 1$, (b)$\tau_s/t_L = 2$, (c)$\tau_s/t_L = 4$, (d)$\tau_s/t_L = 10$

1. Different from the analysis on the stress uniformity of elastic specimen in SHPB tests, the stress uniformity of viscoelastic specimen is not only dependent on the wave impedance ratio R_i and the rise-time τ_s/t_L of incident wave but also on the relaxation time θ_2.

2. Except for the case of short rise-time ($\tau_s/t_L = 1$), the smaller the relaxation time θ_2 is, the later the stress uniformity reaches, but the higher the strain rate is.

3. Except for the case of short rise-time ($\tau_s/t_L = 1$), the smaller the instantaneous wave impedance R_i is, the later the stress uniformity reaches and the lower the strain rate is.

4. Except for the case of short rise-time ($\tau_s/t_L = 1$), the longer the dimensionless rise-time is, the later the stress uniformity reaches. In fact, when the rise-time is $\tau_s/t_L = 2$, it is an optimum choice to achieve the stress uniformity, coinciding with the analysis on the stress uniformity of elastic specimens.

5. Distinguished with the elastic specimen, the strain uniformity and stress uniformity of viscoelastic specimens are not equivalent but different from each other. The strain uniform is earlier to reach than stress uniform at shorter rise-time, but it is contrary when the rise-time becomes longer.

6. The strain rate is non-uniformly distributed along viscoelastic specimens. The average strain rate increases with decreasing θ_2, but decreases with decreasing R_i, and with increasing τ_s/t_L.

Acknowledgements: The authors acknowledge the financial support from the National Natural Science Foundation of China (No. 10032010) and the Science and Technology Funds of China Academy of Engineering Physics (CAEP).

References

[1] H. Kolsky. An investigation of the mechanical properties of materials at very high rates of loading. *Proc. Phys. Soc.*, B62:676–700, 1949.

[2] H. Kolsky. *Stress wave in solids.* Clarendon Pess, 1953.

[3] G. Ravichandran and G. Subhash. Critical appraisal of limiting strain rates for compression testing of ceramics in a split hopkinson pressure bar. *Journal of American Ceramic Society*, 77:263–267, 1994.

[4] B. Song and W. Chen. Split hopkinson pressure bar techniques for characterizing soft materials. *Latin American Journal of Solids and Structures*, 2:113–152, 2005.

[5] Zhiping Tang, Lanqiao Tian, Chao-Hsiang Chu, and Lili Wang. Mechanical behavior of epoxy resin under high strain rates. *Proc. 2nd Nat. Conf. Explosive Mechanics*, pages 4–1–12, 1981. Yangzhou, China.

[6] Lili Wang. *Foundations of Stress Waves*. National Defense Industry Press, Beijing, 2005.

[7] Lili Wang, Shaoqiu Shi, Jiangying Chen, and Dejin Huang. Studies on ZWT non-linear thermo-viscoelastic constitutive relation and its application. *Journal of Ningbo University Natural Science & Engineering Edition*, 13:141–149, 2000.

[8] Lili Wang and Liming Yang. A class of nonlinear viscoelastic constitutive relation of solid polymeric materials. In Wang Lili, Yu Tongxi, and Li Yongchi, editors, *Progress in Impact Dynamics*, page 88, Hefei, China, 1992. The Press of China University of Science and Technology.

[9] L. M. Yang and V. P. W. Shim. An analysis of stress uniformity in split hopkinson bar test specimens. *International Journal of Impact Engineering*, 31(2):129–150, 2005.

[10] U. Zencker and R. Clos. Limiting conditions for compression testing of flat specimens in the split hopkinson pressure bar. *Experimental Mechanics*, 39:343–348, 1999.

[11] Fenghua Zhou. *Study on the Nonlinear Viscoelastic and Damage-Failure Behaviors of PMMA at High Strain-rates and Large Deformation*. University of Science & Technology of China, Hefei, 1990.

[12] Fenghua Zhou, Lili Wang, and Shinsheng Hu. On the effect of non-uniformity in polymer specimen of SHPB tests. *Journal of Experimental Mechanics*, 7(1):23–29, 1992.